RSC Advances

PAPER

View Article Online
View Journal | View Issue

Check for updates

Cite this: *RSC Adv.*, 2025, **15**, 26039

Graphene oxide anchored ferric vanadate acid for the electrochemical detection of bisphenol A in tap water and urine†

Huan Tao,[ab] Feiling Xie,[b] Zhi Li,[*bd] Liangzhuo Qu,[*b] Qingbing Zha[*bc] and Mingshan Zhu[bd]

Received 4th June 2025
Accepted 12th July 2025

DOI: 10.1039/d5ra03944d

rsc.li/rsc-advances

The gradual emissions of bisphenol A (BPA) pose significant health risks by interfering with hormonal regulation, which urgently require to develop an efficient and rapid detection method. Here, an electrochemical sensor using graphene oxide anchored ferric vanadate acid (GO/$FeVO_4$) nanocomposite was developed for BPA detection. The electrochemical signals of GO grafted on $FeVO_4$ was significantly enhanced by 7.4-fold relative to that of pure $FeVO_4$, attributed to transition metal valence effects and adsorption by H-bond. The optimized system achieved a detection limit of 1.18 μM with a linear range of 0.01–40 μM. Additionally, it displayed outstanding stability, reproducibility and selectivity. These findings demonstrate strong potential for environmental monitoring and clinical diagnostics, particularly for rapid on-site BPA detection in tap water and urine. The sensor of GO/$FeVO_4$ with high conductivity and catalytic activity offers a sensitive, cost-effective solution for BPA detection in environmental and medical clinics.

Open Access Article. Published on 22 July 2025. Downloaded on 6/1/2026 6:18:28 PM.
This article is licensed under a Creative Commons Attribution-NonCommercial 3.0 Unported Licence.

1. Introduction

As is known, bisphenol A (BPA), a commonly used plastic monomer, is extensively utilized in food packaging and container manufacturing to effectively protect food from external contamination.[1,2] However, temperature-dependent BPA migration from plastic products during production poses demonstrated risks to human health, including endocrine disruption and developmental toxicity. According to recent investigations, prolonged exposure to BPA has been epidemiologically associated with various adverse health effects, particularly reproductive system disorders, elevated cancer risks, and endocrine disruption. Hence, developing rapid and sensitive BPA detection methods is critical for environmental protection and public health preservation.[3–5]

Currently, various analytical methods such as chemiluminescence, mass spectrometry and liquid chromatography, and gas chromatography-mass spectrometry, have been widely employed for the detection of BPA.[6] Despite the advantages of specificity and accuracy, high-end chromatographic methods face significant limitation including exorbitant prices, complexity of operation, and poor suitability for real-time monitoring.[7–11] Recently, electrochemical sensing technology has gained attention as a potentially effective strategy because of simplified sample preparation, operational ease, high sensitivity and rapid response times.[12–16]

Ferric vanadate acid ($FeVO_4$), a representative two-dimensional material, exhibits an optimal combination of high sensitivity, excellent selectivity, fast response kinetics, remarkable stability, and unique photoelectric properties. These characteristics enable selective molecular recognition capabilities for precise target analyte detection. Recent research results have demonstrated that $FeVO_4$ nanorods exhibit excellent electrochemical response to BPA, indicating its potential as an efficient sensor material for detecting BPA.[17,18] However, the electron transfer capability of $FeVO_4$ is still relatively low, which limits its high sensitivity in electrochemical detection of BPA. Graphene oxide (GO), as an emerging two-dimensional material, possesses lots of advantages including large surface area, high sensitivity, excellent conductivity, drug delivery, and sensing, making it an ideal substance for chemical and biosensors.[19–21] Therefore, grafting GO onto the surface of $FeVO_4$ as an electron bridge accelerates the electron transfer of target molecules to the $FeVO_4$ surface, effectively enhancing the detection sensitivity of GO/$FeVO_4$.

Inspirated by these, herein, taking the specific binding ability of $FeVO_4$ to target molecules, which can change the binding state between itself and target molecules, and the transfer capability of GO, we proposed a GO/$FeVO_4$ nanocomposite-based electrochemical sensor for detecting BPA

[a]*Department of Clinical Laboratory Medical, The First Affiliated Hospital of Jinan University, Guangzhou 510630, China*

[b]*Department of Medical Laboratory, The Fifth Affiliated Hospital of Jinan University (Heyuan Shenhe People's Hospital), Heyuan, 517000, China. E-mail: zhili@jnu.edu.cn; quliangzhuo@163.com; zhaqingbb@sina.com*

[c]*Center of Reproductive Medicine, The First Affiliated Hospital of Jinan University, Guangzhou 510630, China*

[d]*College of Environment and Climate, Jinan University, Guangzhou 511443, China*

† Electronic supplementary information (ESI) available. See DOI: https://doi.org/10.1039/d5ra03944d

© 2025 The Author(s). Published by the Royal Society of Chemistry

Open Access Article. Published on 22 July 2025. Downloaded on 6/1/2026 6:18:28 PM.
This article is licensed under a Creative Commons Attribution-NonCommercial 3.0 Unported Licence.

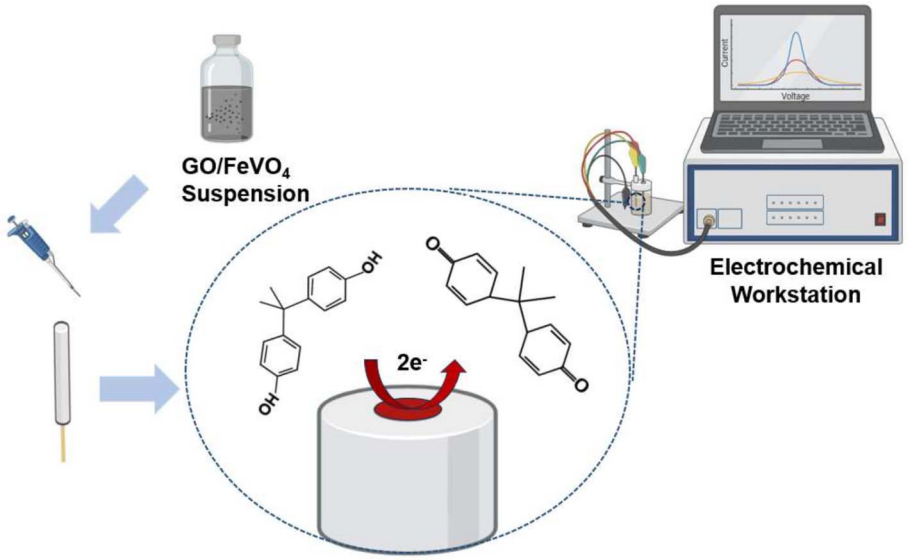

Scheme 1 The GO/$FeVO_4$ electrochemical sensor for BPA detection.

(Scheme 1). The carboxyl and hydroxyl groups on GO sheets could provide binding sites for BPA through H-bonding, and $FeVO_4$ acts as an electron bridge with valence metal effect to accelerate the oxidation of BPA and the rapid transfer of electrons, thereby enhancing the electrochemical sensing signal of BPA. This sensor demonstrates good reproducibility, superior selectivity, stability. These characteristics, combined with its successful application in complex matrices including human urine and tap water, confirm its strong potential for practical environmental and biomedical monitoring.

2. Materials and methods

The instruments, other experiments and characterizations are discussed in ESI.†

2.1. Materials

BPA was sourced from Sigma Chemical Co. Ltd, while GO was procured from Nanjing Xianfen. Sodium dihydrogen phosphate, disodium hydrogen phosphate, potassium ferrocyanide, potassium ferricyanide, ethylene glycol, hydrochloric acid, ethanol, sodium hydroxide, potassium chloride and the supplier of ferric vanadate acid was Sinopharm Chemicals Reagent Co., Ltd in China. Every reagent used were analytical grade, and they were all used immediately without any additional purification.

2.2. Preparation of GO, $FeVO_4$ and GO/$FeVO_4$

2 mg GO was dissolved in a mixture solution of ethanol and water ($V_{water}/V_{ethanol} = 1/1$) for a 30 min ultrasonic dispersion, and was subsequently diluted into 0.02, 0.04, 0.08, 0.12 and 0.2 mg per mL GO solutions. To synthesize GO/$FeVO_4$, 2 mg $FeVO_4$ was added respectively to the different concentrations of GO solutions and sufficiently dissolve through a 30-minute ultrasonic dispersion to obtain 1%, 2%, 4%, 6% and 10% GO/$FeVO_4$ solutions. For comparison, solutions containing GO or $FeVO_4$ alone was prepared with the same method. Then, 5 μL Nafion was added to the above mixed solution.

2.3. Fabrication of GO/$FeVO_4$ sensor

Before preparation, 0.05 mm alumina powder was applied to polish the surface of glassy carbon electrode (GCE) (3 mm in diameter), and then the GCE surface was thoroughly washed with ultrapure water and dried at room temperature. Next, the pretreated GCE was covered with 10 μL of GO/$FeVO_4$ suspension and dried (Scheme 1). For comparison, the GO or $FeVO_4$ sensor were prepared *via* the same procedure.

2.4. Apparatus

Using a standard three-electrode arrangement, a CHI 760 electrochemical workstation was used for all electrochemical measurements. The standard setup included a platinum counter electrode, and a saturated calomel electrode (SCE) as the reference electrode, and the working electrode is a GCE modified by GO/$FeVO_4$. The differential pulse voltammetry (DPV) approach was employed to assess BPA, and the parameters used were as follows: 0.05 s pulse width, 50 mV amplitude, 0–1.2 V potential range, and a 0.004 V additional potential. Cyclic voltammetry (CV) was applied to evaluate the electrochemical characterization of different electrodes under the conditions of 0.001 V interval, −0.4 to 0.8 V potential range, and 100 mV s^{-1} scan rate. Electrochemical impedance spectroscopy (EIS) was carried out with a 5 mV amplitude and the range of frequencies of 1.0–1.0 × 10^5 Hz in 0.1 M KCl solution, which includes 2.5 mM $K_3[Fe(CN)_6]/K_4[Fe(CN)_6]$.

2.5. Pretreatment of real sample

The urine samples were obtained from three healthy volunteers at Department of Clinical Laboratory Medical, The First Affiliated Hospital of Jinan University (Guangzhou, China). Each

© 2025 The Author(s). Published by the Royal Society of Chemistry

Open Access Article. Published on 22 July 2025. Downloaded on 6/1/2026 6:18:28 PM.
This article is licensed under a Creative Commons Attribution-NonCommercial 3.0 Unported Licence.

research participant signed a written informed consent form in accordance with the Declaration of Helsinki. According to the "Ethical Review Method for Life Science and Medical Research Involving Humans" in China, this study does not require further ethical approval from the ethics committee, as its purpose does not involve the exploration of human diseases or any potentially heritable genetic manipulation. Tap water was collected at the laboratory of The First Affiliated Hospital of Jinan University. These real sample was stored at 4 °C and then they were centrifuged at 8000 rpm to obtain the supernatant. The supernatant was further diluted 10-fold with 0.1 M phosphate buffer (pH = 7.0) to prepare a standard solution for subsequent electrochemical testing. DPV technique was adopted for the BPA detection in real sample, and the standard spiking method was applied to evaluate the recovery rates of BPA at concentrations of 2, 4, and 6 μM in real samples.

3. Results and discussion

3.1. Physical characterizations

The morphologies of $FeVO_4$, GO and GO/$FeVO_4$ were observed by transmission electron microscopy (TEM), which was presented as the one-dimensional belt-like shape, respectively (Fig. 1a–c).[22] The XRD pattern was used to characterize the chemical makeup of the produced GO, $FeVO_4$, and GO/$FeVO_4$ in Fig. 1d. The prepared GO sheet exhibited a prominent peak at 10.2°, which is in excellent alignment with the values stated in the literature.[23,24] The $FeVO_4$ sample was synthesized through a straightforward hydrothermal method (Fig. 1d), displaying some weak diffraction peaks, indicating its low crystallinity. The XRD analysis of the calcined sample was precisely matched to triclinic $FeVO_4$ (PDF #71-1592), consistent with previous reports.[25] The result demonstrated GO incorporation did not change the $FeVO_4$ crystal structure.

Additionally, the surface valence states and elemental composition of $FeVO_4$ nanobelts were investigated using X-ray photoelectron spectroscopy (XPS). Fig. 1e shows the Fe 2p spectrum, and there were six peaks found. Two peaks at 711.51 eV and 724.10 eV show Fe $2p_{3/2}$ and Fe $2p_{1/2}$, respectively, indicating that Fe^{2+} is one of the Fe species found on the nanobelts. As seen in (Fig. 1f), the presence of Fe^{3+} species is confirmed by two further peaks at 714.27 eV and 726.51 eV, and two satellite peaks at 719.69 eV and 733.41 eV, V $2p_{3/2}$ and V $2p_{1/2}$ are responsible for the peaks at 517.12 eV and 530.15 eV, respectively. According to this discovery, vanadium can be found on the surface of the nanobelt in two valence states: pentavalent (V^{5+}) and tetravalent (V^{4+}). The presence of low-valence Fe/V species on $FeVO_4$ can be attributed to the reaction between $FeCl_3$ and NH_4VO_3 under high temperature and pressure, which releases ammonia. Acting as a reducing agent, ammonia converts some of the low-valence Fe^{2+}/V^{4+} species from the high-valence Fe^{3+}/V^{5+}species.[26]

3.2. Electrochemical characterization

CV analysis was used to compare and analyze the electrochemical performance and electron transport properties of the four suggested sensors (Fig. 2a). The results showed that the GCE electrode displayed the weakest redox peak signal, which can be enhanced by GO and $FeVO_4$, respectively. Notably, the GO/$FeVO_4$ sensor, where GO and $FeVO_4$ were simultaneously added on the GCE electrode, showed the highest redox peak,

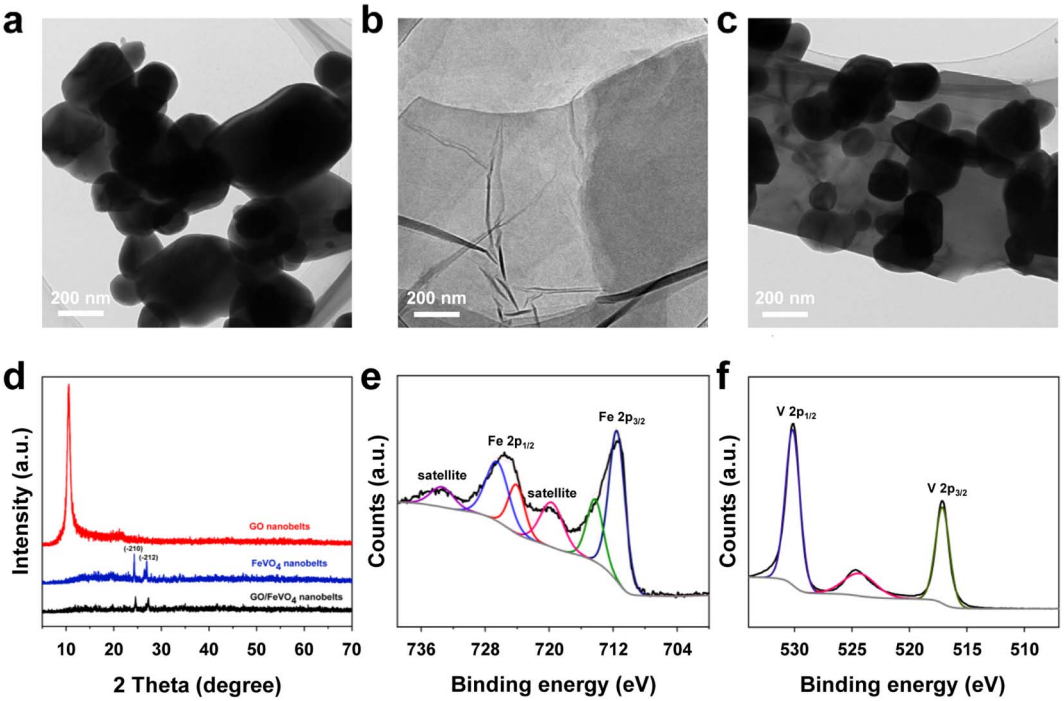

Fig. 1 TEM images of $FeVO_4$ (a), GO (b) and GO/$FeVO_4$ (c); XRD patterns (d) of $FeVO_4$; Fe 2p (e) and V 2p (f) spectra of $FeVO_4$.

Open Access Article. Published on 22 July 2025. Downloaded on 6/1/2026 6:18:28 PM.
This article is licensed under a Creative Commons Attribution-NonCommercial 3.0 Unported Licence.

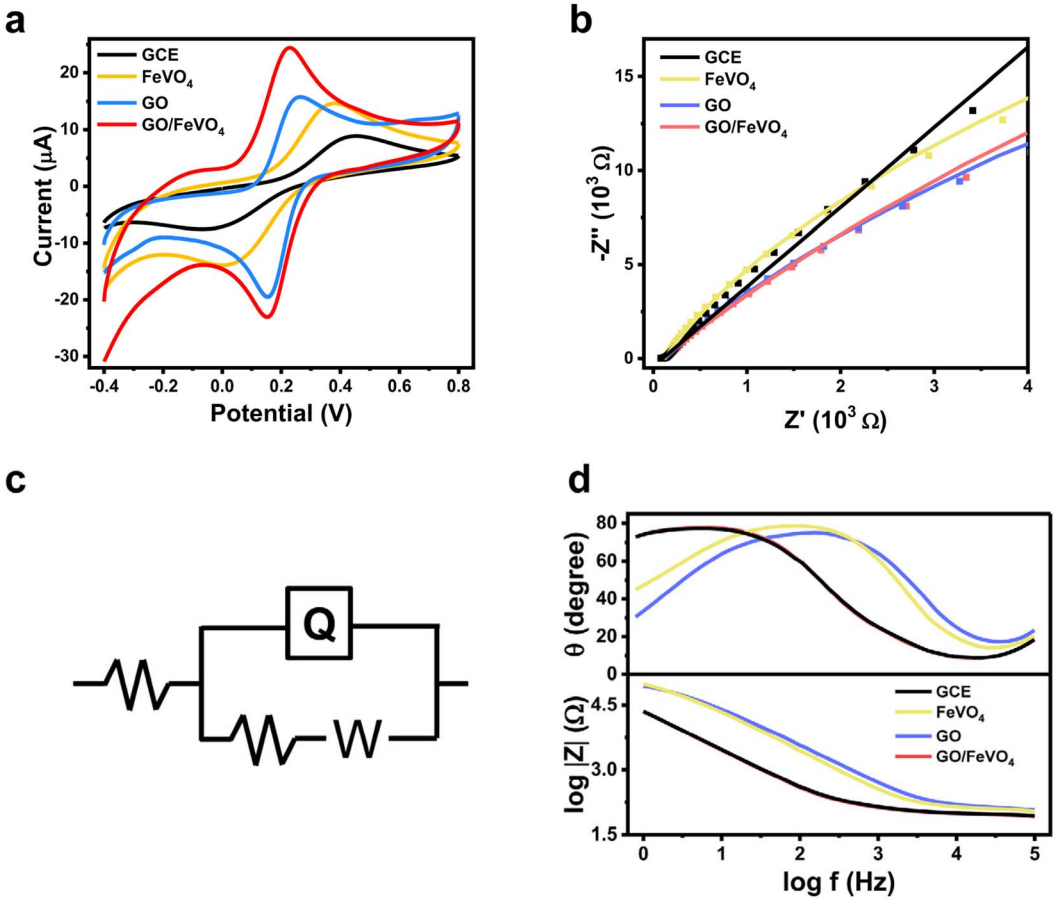

Fig. 2 CVs (a), Nyquist plots (b), equivalent circuit (c) and Bode plots (d) of GCE, $FeVO_4$, GO and GO/$FeVO_4$ in a 2.5 mM $K_3[Fe(CN)_6]/K_4[Fe(CN)_6]$ solution containing 0.1 M KCl. Equivalent circuit was used for simulating EIS.

indicating that the modification by GO can effectively improve the electronic transmission ability of $FeVO_4$. The electron transport on the electrode surfaces of a few sensors was investigated with EIS.[27] The electrical impedance of four sensors were represented by the Nyquist diagram (Fig. 2b). The radius is typically used to illustrate the charge transfer resistance, a smaller radius denotes a lower resistance.[28,29] The GO sensor has the smallest electrical impedance value, followed by GO/$FeVO_4$, $FeVO_4$ and GCE sensors. The EIS data was further fitted to acquire the equivalent circuit diagram (Fig. 2c). In the Fig. 2d, the Bode plots were also examined to evaluate the capacity of the sample for charge transfer resistance. As the impedance value increases, log|Z| increases in the Bode-magnitude plot.[30–34] As a result, the GO/$FeVO_4$ electrode exhibited a faster electron transport capability compared to the GO electrode, with similar trends observed in the Bode-phase plot. Based on these findings, the GO/$FeVO_4$ electrode shows great promise as a superior electrochemical sensing material.

3.3. Electrochemical detection of BPA

The electrochemical behavior of 20 μM BPA in 0.1 M phosphate buffer (pH = 7.0) for four various electrodes was reflected by DPV method (Fig. 3a). BPA showed a comparatively consistent oxidation peak potential for the GO/$FeVO_4$ sensor at 0.512 V. Compared with GCE, $FeVO_4$ and GO electrodes, the peak current signal of GO/$FeVO_4$ for BPA is improved 9.0, 7.4 and 2.8 times (Fig. 3b), respectively. This can be ascribed to the remarkable electrocatalytic activity of GO, which accelerates the electron transport of $FeVO_4$ for BPA detection. Additionally, the porous structure of $FeVO_4$ affords the GO nanosheets a large number of attachment sites.[35] These results indicate that the GO/$FeVO_4$ sensor has outstanding BPA detection capabilities.

3.4. GO/$FeVO_4$ electrode ideal conditions

For the determination of optimal detection conditions of GO/$FeVO_4$ electrode, a series of parameters including content percentage, time, accumulation potential and pH value were investigated with DPV method. Firstly, the content of GO on GO/$FeVO_4$ electrode is one of the important factors for BPA detection. From 1 to 6%, as the GO concentration increased, the peak current gradually rose; however, it sharply decreased when the GO content reached 10%. This drop is attributed to the excessive GO, which obstructed the active sites of $FeVO_4$ (Fig. 4a). Therefore, 6% GO was chosen as the optimal content for BPA detection. In addition, the phosphate buffer at a certain pH level can have a significant impact on BPA detection (Fig. 4b). The

© 2025 The Author(s). Published by the Royal Society of Chemistry

Open Access Article. Published on 22 July 2025. Downloaded on 6/1/2026 6:18:28 PM.
This article is licensed under a Creative Commons Attribution-NonCommercial 3.0 Unported Licence.

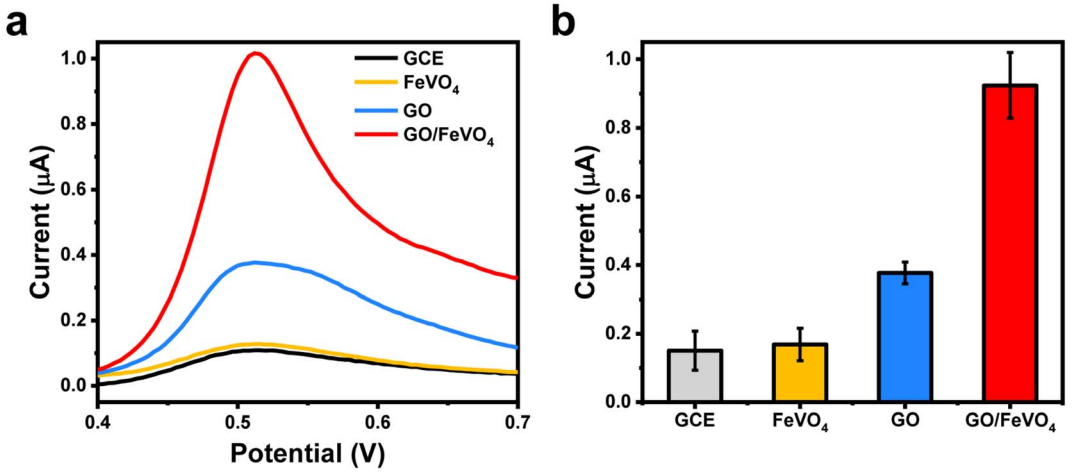

Fig. 3 The DPVs (a) and matching histograms (b) for different sensors in a 0.1 M phosphate buffer (pH = 7.0) solution.

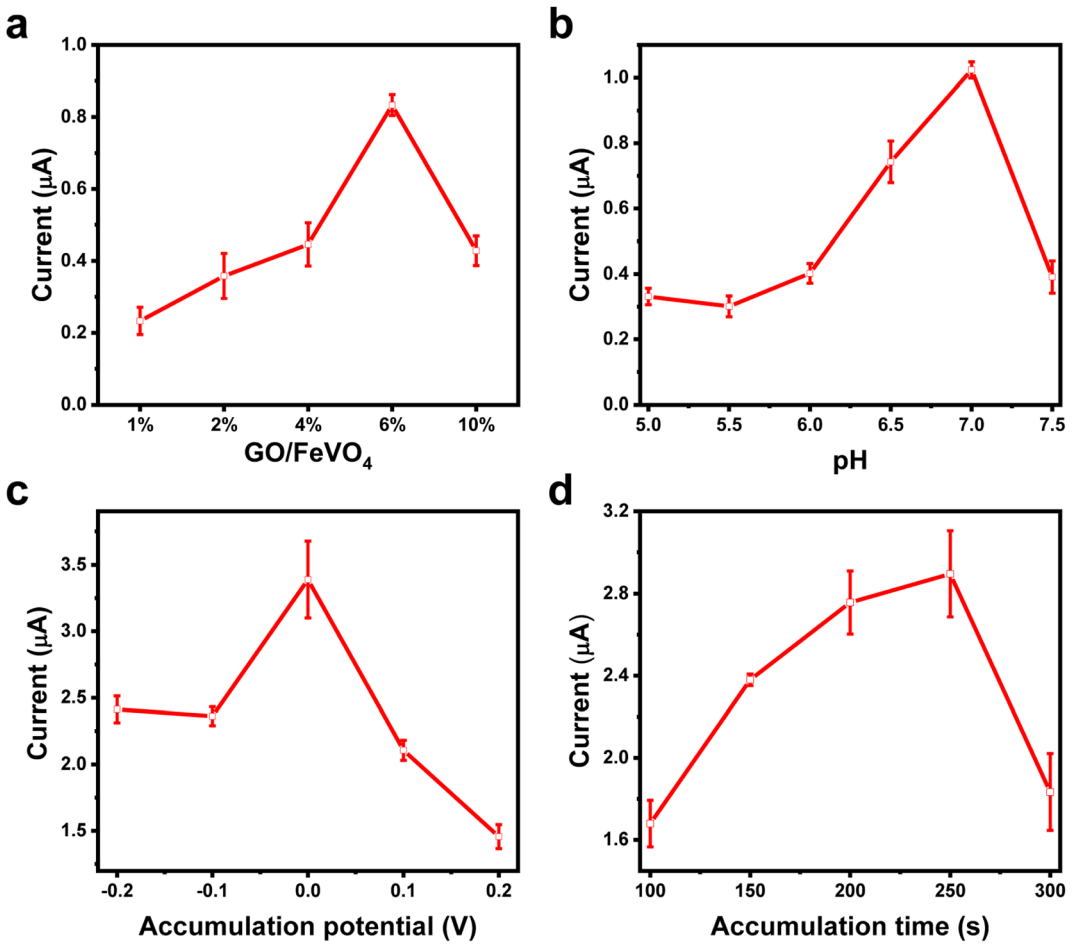

Fig. 4 The impact of various weight ratios of $GO/FeVO_4$ (a), pH value (b), accumulation potential (c), and accumulation time (d) on the 20 μM BPA peak current in 0.1 M phosphate buffer (pH = 7.0) was studied using the $GO/FeVO_4$ sensor.

peak current of BPA was measured at different pH level range from 5.0–7.5, and the results showed that BPA has the highest current value when pH is 7.0. As a result, a phosphate buffer solution with a pH of 7.0 was selected as a prerequisite for the ensuing detection procedure. Additionally, the accumulation potential and the accumulation time are also critical factors in the electrochemical detection of BPA (Fig. 4c and d). The peak current of BPA was changed at different accumulation potential (−0.2–0.2 V) and accumulation time (100–300 s). The results of the study showed that BPA exhibited the maximum peak

© 2025 The Author(s). Published by the Royal Society of Chemistry

Open Access Article. Published on 22 July 2025. Downloaded on 6/1/2026 6:18:28 PM.
This article is licensed under a Creative Commons Attribution-NonCommercial 3.0 Unported Licence.

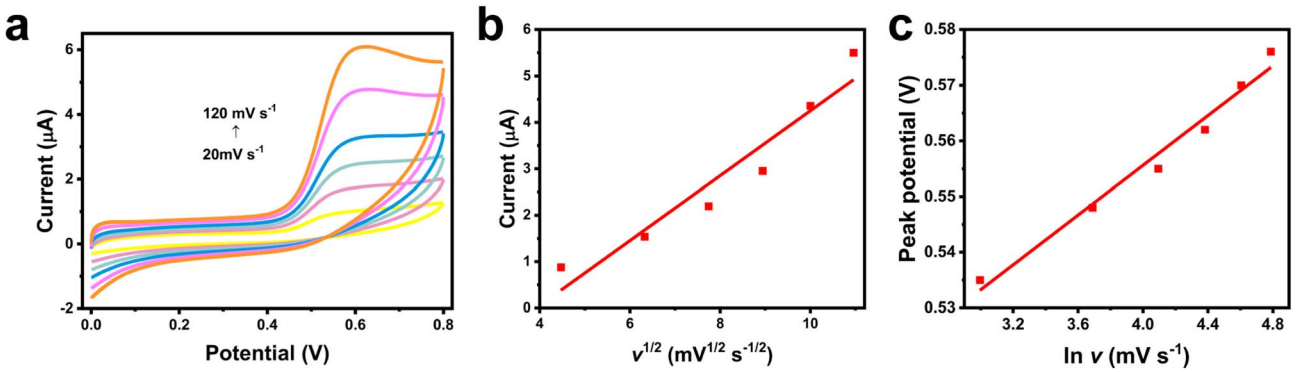

Fig. 5 CVs (a) of 20 μM BPA detected by the GO/$FeVO_4$ electrode in 0.1 M phosphate buffer (pH = 7.0) at different scan rate from 20 to 120 mV s^{-1}. The correlation between peak currents (I_{pa}) and $v^{1/2}$ ($mV^{1/2}$ $s^{-1/2}$) (b). The correlation of peak potential and Napierian logarithm of scan rate (ln v) (c).

current at 250 s (Fig. 4d) and 0 V (Fig. 4c) accumulation potentials.

3.5. Effect of scan rate

In order to uncover the oxidation mechanism at GO/$FeVO_4$-sensor for BPA detection, the impact of scan rate were explored by CV technique. With the increase of scan rate, the value of the BPA oxidation peak current gradually increases (Fig. 5a), and a linear correlation between the square root of the scanning rate, as well as the peak current was found (Fig. 5b), which can be represented by the following equation: I_{pa} (μA) = (0.6997 ± 0.10)$v^{1/2}$ ($mV^{1/2}$ $s^{-1/2}$) − (2.7462 ± 0.8367), with an R^2 value of 0.9056. The outcome shows diffusion regulates the BPA electrochemical response at the GO/$FeVO_4$ sensor surface. Furthermore, as the scan rate raised, the oxidation peak potentials (E_{pa}) moved favorably. The relationship between the Napierian logarithm of E_{pa} and v (ln v) is linear, as shown in Fig. 5c, and can be described by the equation: E_{pa} (V) = (0.0224 ± 0.0017)ln v (mV s^{-1}) + (0.4662 ± 0.0069), with an R^2 value of 0.9729.

The following formula defines E for diffusion-controlled and irreversible electrode operations:[36]

$$E = E^{\theta} + (RT/anF)\ln(RTk^{\theta}/anF) + (RT/anF)\ln v$$

In this formula, the variables E^{θ}, R, T, a, n, F, k^{θ}, and v denote the formal redox potential, the gas constant, the absolute temperature, transfer coefficient, the number of electrons involved in the reaction, the Faraday constant, the standard rate constant of

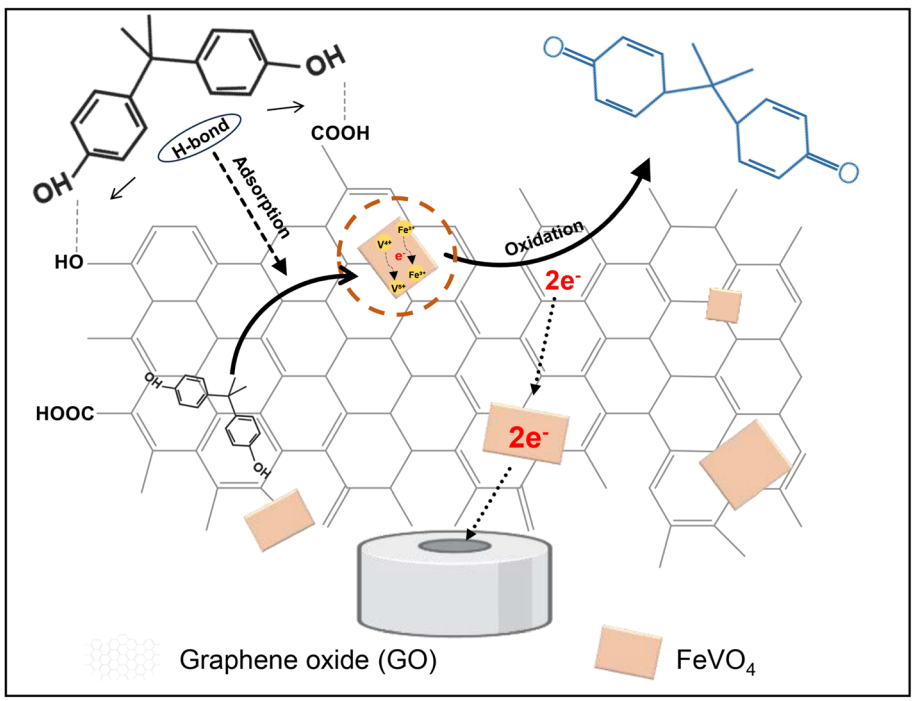

Scheme 2 BPA detection reaction mechanism at the GO/$FeVO_4$ sensor.

© 2025 The Author(s). Published by the Royal Society of Chemistry

Open Access Article. Published on 22 July 2025. Downloaded on 6/1/2026 6:18:28 PM.
This article is licensed under a Creative Commons Attribution-NonCommercial 3.0 Unported Licence.

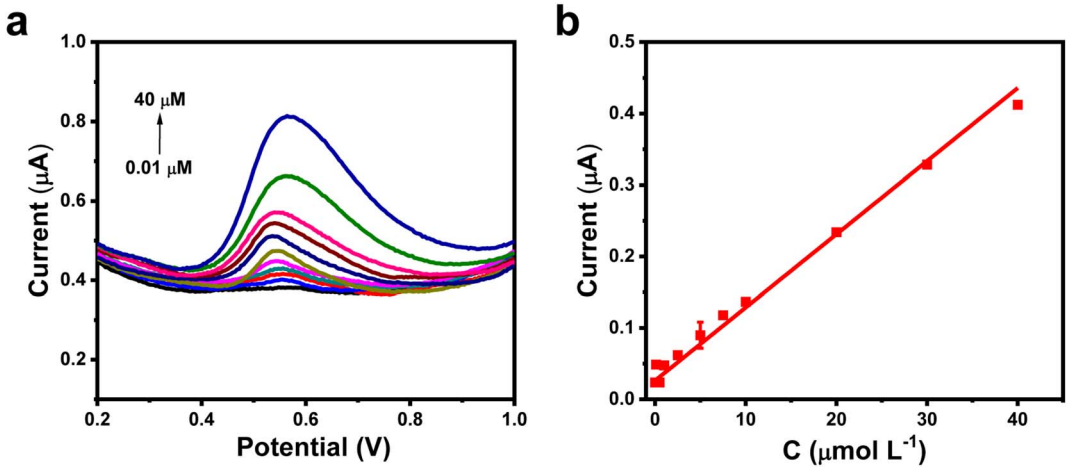

Fig. 6 DPVs for various BPA concentrations in 0.1 M phosphate buffer (pH = 7.0) at the GO/$FeVO_4$ sensor (a). Linear relationships between the oxidation peak currents and the concentrations of BPA (b).

the reaction, and the scan rate, respectively. Consequently, the slope in Fig. 5c corresponds to RT/anF. The value of n was determined to be 2.29 (with $F = 96\,480$, $R = 8.314$, and $T = 298$), assuming that for an irreversible process, $a = 0.5$. These findings demonstrate that the electrochemical detection of BPA at the GO/$FeVO_4$ sensor surface involves the conversion of two electrons to two protons.[37] Scheme 2 suggests a potential response mechanism based on the aforementioned findings. Firstly, the carboxyl and hydroxyl groups on GO sheets may provide binding sites for BPA through hydrogen bonding,[38] GO adsorbs onto the surface of BPA, and an oxidation–reduction reaction occurs under electrochemical influence, generating

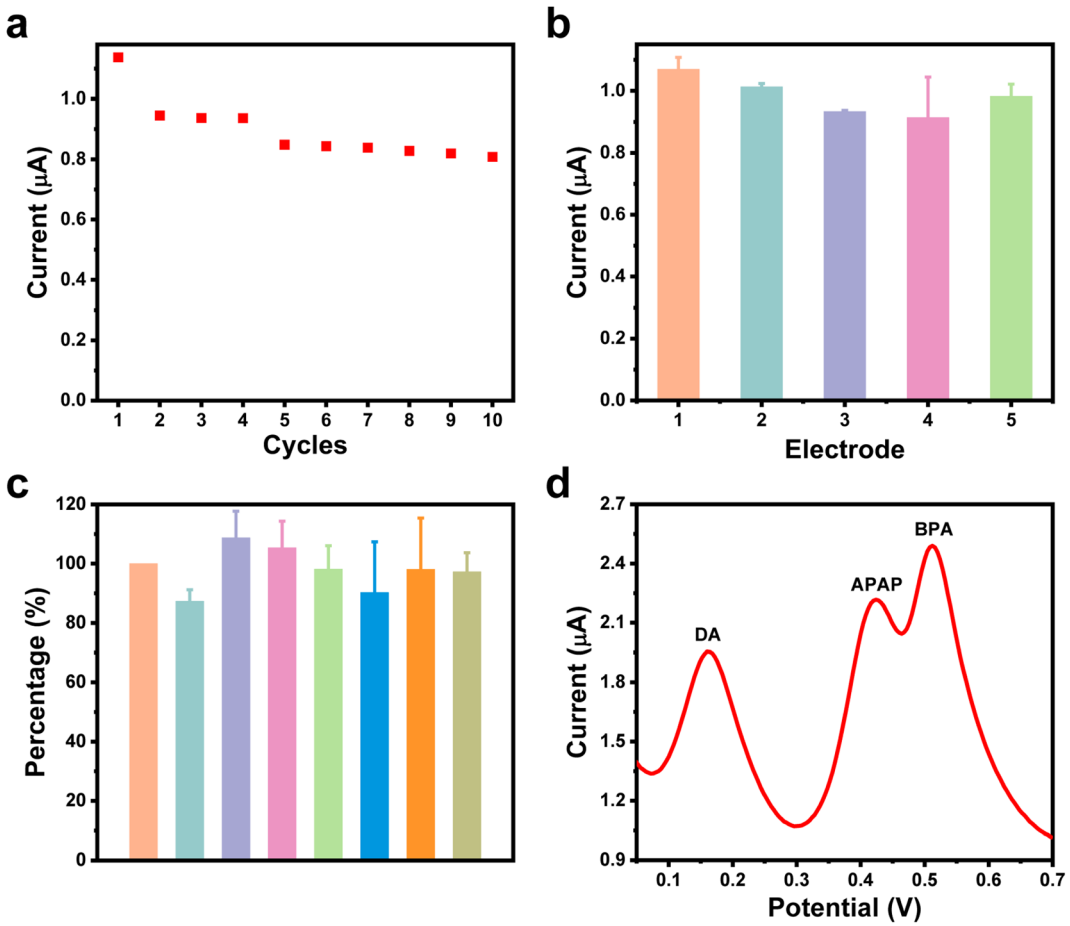

Fig. 7 The stability (a), reproducibility (b), anti-interference (c) and selectivity (d) of the GO/$FeVO_4$ sensor in 0.1 M phosphate buffer (pH = 7.0).

Open Access Article. Published on 22 July 2025. Downloaded on 6/1/2026 6:18:28 PM. This article is licensed under a Creative Commons Attribution-NonCommercial 3.0 Unported Licence.

electrons. Then these electrons are rapidly transmitted to the surface of GCE through the highly conductive GO/$FeVO_4$ hybrid network, where $FeVO_4$ acts as an electron bridge with mixed-valence states (Fe^{2+}/V^{4+} and Fe^{3+}/V^{5+}).[39] This efficient electron transfer results in the generation of a well-defined electrochemical signal in the electrochemical workstation, enabling the highly sensitive and selective quantitative and qualitative detection of BPA.

3.6. Detection of BPA at GO/$FeVO_4$ sensor

The DPV approach was used to measure the various BPA concentrations found by the GO/$FeVO_4$ electrode under optimal experimental circumstances (Fig. 6a and b). From 0.01–40 μM, the oxidation peak currents elevated with the increase of BPA concentration. Furthermore, the following equation illustrates a linear relationship between the corresponding peak current and the BPA concentration: I_{pa} (μA) = (0.0102 ± 0.00000059)C (μM) + (0.0262 ± 0.000058), R^2 = 0.992. The detection limit (LOD = $3s_b/S$) of BPA is calculated to be 1.18 μM (Table S1†), where S is the slope with the standard curve or the sensitivity for the electrochemical sensor platform, and s_b is the standard deviation of the blank.[40] In comparison to previous studies, the current GO/$FeVO_4$ sensor display the lowest LOD for the electrochemical identification of BPA (Table S2†).

3.7. Reproducibility and selectivity studies

The stability of the GO/$FeVO_4$ electrode was evaluated through ten consecutive scans by DPV technique. After 10 consecutive tests, the electrochemical signal of BPA still kept 71% of the first cycle, which suggests GO/$FeVO_4$ sensor with excellent stability (Fig. 7a). To determine the reproducibility of the GO/$FeVO_4$ sensor, 5 electrodes of GO/$FeVO_4$ were independently used for BPA detection with a standard deviation (S.D.) of 6.2% (Fig. 7b and Table S3†), demonstrating that the GO/$FeVO_4$ sensor has good reproducibility performance for BPA detection. In addition, in Fig. 7c, the BPA oxidation peak current value was recorded after adding various interferers, including NaCl, Glu, KCl, KBr, dopamine (DA), acetaminophen (APAP) and tetrabromobisphenol A (TBBPA) in 0.1 M phosphate buffer (pH = 7.0). The S.D. of BPA in the presence of interfering species were 3.0%, 3.2%, 3.3%, 3.6%, 7.6%, 8.6%, and 2.9%, respectively (Table S4†). These results highlight the excellent interference resistance of the GO/$FeVO_4$ sensor, with all S.D. values remaining below 9.0%. The selectivity of this sensor was measured by DPV in 0.1 M phosphate buffer (pH = 7.0), which includes 40 μM DA solution, 30 μM BPA and 50 μM APAP (Fig. 7d).

Table 1 BPA detection in actual samples

Sample	Added (μM)	Found (μM)	Recovery (%)
Urine	2	2.30	110.1%
	4	4.19	104.7%
	6	5.92	98.8%
Tap water	2	2.06	103%
	4	4	100.2%
	6	6.1	101.9%

3.8. Detection of real sample

To detect practicability of the designed GO/$FeVO_4$ sensor, actual samples from human urine and tap water were collected to detect the level of BPA. Initially, a linear relationship between peak current and BPA concentrations in 0.1 M phosphate buffer (pH = 7.0) was established (Fig. S1†), which can be represented as: I_{pa} (μA) = (0.01657 ± 0.00205)C_{BPA} (μM) − (0.00523 ± 0.0082), R^2 = 0.9553. The standard addition method was used to analyze BPA by DPV method in urine and tap water. Furthermore, the recovery rates of BPA were calculated using the equation mentioned above. According to Table 1, the recovery rates range from approximately 90% to 110%, suggesting that this sensor may be used to accurately assess BPA levels in real samples (Table 1).

4. Conclusions

A new ultra-sensitive electrochemical sensor with GO anchored $FeVO_4$ for detecting BPA has been developed. The carboxyl and hydroxyl groups on GO sheets may provide binding sites for BPA through H-bonding, and $FeVO_4$ acts as an electron bridge with valence metal effect to accelerate the oxidation of BPA and the rapid transfer of electrons, thereby enhancing the electrochemical sensing signal of BPA. The GO/$FeVO_4$ sensor displays a wide linear range and a low detection limit, along with outstanding reproducibility, anti-interference ability, selectivity, and stability. In addition, it was successfully used for the detection of real samples in tap water and urine. These findings suggest that the GO/$FeVO_4$ sensor is a potential electrochemical platform for convenient, simple, and highly effective electrochemical detection for tracking endocrine disruptors, which can be extended to the analysis of environmental contaminants.

Data availability

Data will be made available on request.

Author contributions

H. T.: methodology, investigation, formal analysis, writing—original draft. F. X.: formal analysis, data curation, writing—original draft. Z. L.: conceptualization, writing—review and editing. L. Q.: writing—review and editing, supervision. Q. Z.: conceptualization, writing—review and editing, supervision, funding acquisition. M. Z.: supervision. All authors have read and agreed to the published version of the manuscript.

Conflicts of interest

The authors declare no conflicts of interest.

© 2025 The Author(s). Published by the Royal Society of Chemistry

Open Access Article. Published on 22 July 2025. Downloaded on 6/1/2026 6:18:28 PM. This article is licensed under a Creative Commons Attribution-NonCommercial 3.0 Unported Licence.

Acknowledgements

This work supported by the Science and Technology Project of Heyuan, China Social Development and Rural Science (No. 2023008) and the Project of Guangdong Administration of Traditional Chinese Medicine (No. 20232177).

References

1 G. A. Idowu, T. L. David and A. M. Idowu, *Mar. Pollut. Bull.*, 2022, **176**, 113444.
2 M. K. Fuzak and A. Z. Pollack, *Semin. Reprod. Med.*, 2024, **42**, 274–287.
3 A. E. Peters, E. A. Ford, S. D. Roman, E. G. Bromfield, B. Nixon, K. G. Pringle and J. M. Sutherland, *Hum. Reprod. Update*, 2024, **30**, 653–691.
4 S. Zhou, X. Wang, Y. Huang, Y. Liu, Y. Zheng, P. Chu, L. Zhu and X. Xu, *Mar. Pollut. Bull.*, 2024, **208**, 117058.
5 J. Liu, L. Zhang, G. Lu, R. Jiang, Z. Yan and Y. Li, *Ecotoxicol. Environ. Saf.*, 2021, **208**, 111481.
6 W. Sun, Y. Qi, L. Wang, Y. Tan, X. Zhang, J. Wang and Y. Li, *Spectrochim. Acta, Part A*, 2025, **327**, 125318.
7 M. Zhang, Y. Sun, Q. Yang and Y. Chen, *Surf. Interfaces*, 2025, **58**, 105851.
8 Ş. Yılmaz, *Surf. Interfaces*, 2022, **32**, 102171.
9 J.-Y. Hu, Z. Li, C.-Y. Zhai, J.-F. Wang, L.-X. Zeng and M.-S. Zhu, *Rare Met.*, 2021, **40**, 1727–1737.
10 N. Akbari, B. Basaran, M. Ghazi-Khansari, B. Akbari-Adergani, A. Bakhtiyari, P. Shavali-gilani and P. Sadighara, *Microchem. J.*, 2024, **207**, 111724.
11 K. Alagumalai, R. Shanmugam, S.-M. Chen, T.-W. Chen, A. M. Al-Mohaimeed, W. A. Al-onazi and M. S. Elshikh, *Surf. Interfaces*, 2021, **23**, 101019.
12 M. L. Báez, A. García, I. Martínez, C. González, M. Gómez and B. Rodríguez, *Int. J. Electrochem. Sci.*, 2024, **19**, 100538.
13 Z. Zhou, J. Han, J. Shao, N. Li, T. Ren, D. Chen and J. Lu, *Surf. Interfaces*, 2025, **60**, 106051.
14 S. Mo, Z. Wang, D. Ding, Z. Yan, Y. Dai, J. Zhang, H. Liu, T. Liang, J. Tong, Z. Li and X. Wang, *Chin. Chem. Lett.*, 2025, **36**, 110190.
15 Y. Wang, R. Zeng, S. Tian, S. Chen, Z. Bi, D. Tang and D. Knopp, *Anal. Chem.*, 2024, **96**, 13663–13671.
16 R. Zeng, M. Qiu, Q. Wan, Z. Huang, X. Liu, D. Tang and D. Knopp, *Anal. Chem.*, 2022, **94**, 15155–15161.
17 M. Javad Javid-Naderi, N. Valizadeh, B. Banimohamad-Shotorbani, M. Shahgolzari, F. Shayegh, R. Maleki-baladi, S. Sargazi and S. Fathi-karkan, *Inorg. Chem. Commun.*, 2023, **157**, 111423.
18 W. Yang, W. Yang, Y. Huang, C. Xu, L. Dong and X. Peng, *Chin. Chem. Lett.*, 2022, **33**, 4628–4634.
19 A. U. Alam and M. J. Deen, *Anal. Chem.*, 2020, **92**, 5532–5539.
20 G. Cai, Z. Yu, R. Ren and D. Tang, *ACS Sens.*, 2018, **3**, 632–639.
21 R. Zeng, Z. Luo, L. Zhang and D. Tang, *Anal. Chem.*, 2018, **90**, 12299–12306.
22 J. Hu, C. Zhai, L. Zeng, Y. Du and M. Zhu, *Catal. Sci. Technol.*, 2018, **8**, 3562–3571.
23 D. Ghosh, S. Mehra, S. Sahay, P. K. Singh and S. K. Maji, *Int. J. Biol. Macromol.*, 2017, **100**, 37–54.
24 P. Viprya, D. Kumar and S. Kowshik, *Proc. Eng.*, 2023, **59**, 84.
25 C. Wang, C. Jin, T. Wang, Z. Liang, F. Xie and Y. Chang, *Mater. Lett.*, 2025, **378**, 137637.
26 B. Patella, M. Buscetta, S. Di Vincenzo, M. Ferraro, G. Aiello, C. Sunseri, E. Pace, R. Inguanta and C. Cipollina, *Sens. Actuators, B*, 2021, **327**, 128901.
27 P. Devi, C. Sharma, P. Kumar, M. Kumar, B. K. Bansod, M. K. Nayak and M. L. Singla, *J. Hazard. Mater.*, 2017, **322**, 85–94.
28 J. Chen, P. Tong, L. Huang, Z. Yu and D. Tang, *Electrochim. Acta*, 2019, **319**, 375–381.
29 Z. Qiu, D. Tang, J. Shu, G. Chen and D. Tang, *Biosens. Bioelectron.*, 2016, **75**, 108–115.
30 S. Ahmad, M. H. Ayoub, A. M. Khan, A. Waseem, M. Yasir, M. S. Khan, T. M. Bajwa and A. J. Shaikh, *Colloids Surf., A*, 2022, **647**, 129057.
31 L. Meng, R. Guo, X. Sun, F. Li, J. Peng, C. Chen, T. Li and J. Deng, *Ceram. Int.*, 2020, **46**, 21360–21366.
32 M. A. Awad, A. A. Hendi, S. Natarajan, K. M. O. Ortashi, S. S. A. Alsaif, R. A. Alnamlah, A. Rasheed and H. Althobaiti, *J. King Saud Univ., Sci.*, 2023, **35**, 102857.
33 Y. Ou, R. Zhu, J. Peng, J. Gao, F. Zhang, M. Hojamberdiev and G. Zhu, *Appl. Nanosci.*, 2021, **13**, 465–474.
34 P. Kamedulski, M. Skorupska, P. Binkowski, W. Arendarska, A. Ilnicka and J. P. Lukaszewicz, *Sci. Rep.*, 2021, **11**, 22054.
35 W. Wang, Y. Zhang, X. Huang and Y. Bi, *J. Mater. Chem. A*, 2019, **7**, 10949–10953.
36 N. Boulanger, A. S. Kuzenkova, A. Iakunkov, A. Nordenström, A. Y. Romanchuk, A. L. Trigub, P. V. Zasimov, M. Prodana, M. Enachescu, S. Bauters, L. Amidani, K. O. Kvashnina, S. N. Kalmykov and A. V. Talyzin, *Adv. Mater. Interfaces*, 2022, **9**, 2200510.
37 Y. Tian, Z. Yu, L. Cao, X. L. Zhang, C. Sun and D.-W. Wang, *J. Energy Chem.*, 2021, **55**, 323–344.
38 T. S. Silva, M. F. R. Bihain, A. K. dos Santos Pereira and D. H. Pereira, *J. Nanopart. Res.*, 2025, **27**, 1–14.
39 J. Zhang, W. Zhao, Z. Li, G. Lu and M. Zhu, *Chem. Eng. J.*, 2021, **403**, 126384.
40 Y. Li, F. Zhang, Z. Li, L. Sun, Z. Wang, P. Li, Y. Sun, J. Ren, Y. Wang and M. Cribb, *Atmos. Res.*, 2017, **188**, 80–89.

© 2025 The Author(s). Published by the Royal Society of Chemistry